Journal Pre-proofs

Multiple phase change-stimulated shape memory and self-healing epoxy composites with thermal regulation function

Zhaowen Huang, Qin Ye, Zijian Shi, Jiao-Ning Tang, Xing Ouyang, Da-Zhu Chen

PII: S1385-8947(20)33506-3
DOI: https://doi.org/10.1016/j.cej.2020.127382
Reference: CEJ 127382

To appear in: *Chemical Engineering Journal*

Received Date: 8 July 2020
Revised Date: 28 September 2020
Accepted Date: 12 October 2020

Please cite this article as: Z. Huang, Q. Ye, Z. Shi, J-N. Tang, X. Ouyang, D-Z. Chen, Multiple phase change-stimulated shape memory and self-healing epoxy composites with thermal regulation function, *Chemical Engineering Journal* (2020), doi: https://doi.org/10.1016/j.cej.2020.127382

This is a PDF file of an article that has undergone enhancements after acceptance, such as the addition of a cover page and metadata, and formatting for readability, but it is not yet the definitive version of record. This version will undergo additional copyediting, typesetting and review before it is published in its final form, but we are providing this version to give early visibility of the article. Please note that, during the production process, errors may be discovered which could affect the content, and all legal disclaimers that apply to the journal pertain.

© 2020 Elsevier B.V. All rights reserved.

Journal Pre-proofs

Multiple phase change-stimulated shape memory and self-healing epoxy composites with thermal regulation function

Zhaowen Huang, Qin Ye, Zijian Shi, Jiao-Ning Tang, Xing Ouyang and Da-Zhu Chen*

Shenzhen Key Laboratory of Polymer Science and Technology, Guangdong Research Center for Interfacial Engineering of Functional Materials, College of Materials Science and Engineering, Shenzhen University, Shenzhen 518060, P.R. China.

* Corresponding Author.

E-mail address: dzchen@szu.edu.cn (D.-Z. Chen)

Journal Pre-proofs

ABSTRACT

Form-stable phase change materials (FSPCMs) are widely used for cost-effective thermal management and energy storage applications. However, the strong rigidity of most FSPCMs at low temperatures and the weak resistance of them to damages when the temperature is exceeding their phase transition points have hindered their installations in limited places. Herein, we developed a novel kind of thermal regulation FSPCM possessing multiple phase change-stimulated shape memory and self-healing properties to address these issues. The synthesis of the FSPCMs are based on confining ethylene glycole distearate (EGDS) within the epoxy-based polymer matrix through photo-initiated polymerization. This strategy, on one hand, prevent the leakage of the liquid EGDS in macroscales, and on the other hand, maintain the mobility of the flowing EGDS in micro-scale regions to allow the FSPCM to perform shape deformation and recovery and enable self-repairing effects through solid-liquid phase transitions. Notably, the polymer matrix in the FSPCM consists of pre-grafted crystalline segments of stearic acid (SA) which improve the compatibility between the matrix and EGDS, and impart the FSPCM with multiple phase transitions to realize stepwise control of the shape memory behaviors. The resulting composite FSPCM also demonstrate good thermal regulation performance and high thermal reliability, which can be promisingly engineered into thermal management of integrated circuits and building glazing system with thermal regulation purpose.

KEY WORDS

Form-stable phase change material

Controllable shape memory

Self-healing

Thermal regulation

Journal Pre-proofs

1. Introduction

Phase change materials (PCMs) can absorb energy during melting and release energy during crystallization in a way that can be used for storage of thermal energy, e.g., to improve utilization efficiency of solar radiation [1] and industrial waste heat [2], or for thermal regulation of buildings [3] and electronic components [4]. Currently, more than 50 products based on PCMs can be found in the market. Most of them are based on organic solid-liquid PCMs due to their varied and adjustable phase change temperature, high latent heat storage density, robust chemical and thermal stability, corrosion resistance, nontoxicity, and low cost [5, 6]. However, during the solid-liquid phase transitions of organic PCMs, the flowing materials are inevitably generated and very difficult to handle. The resulting leakage issue is a long-standing bottleneck for the broad-scale applications of PCMs [7]. Efficient energy storage and thermal regulation using PCMs require suitable encapsulation structures to impart PCMs with form-stable property.

Confining PCMs in core-shell structure and porous framework are the most frequent used strategies to fabricate form-stable phase change materials (FSPCMs) [8]. Microcapsules with PCM as the core and protective material as the shell can bring about favourable properties, such as prevention of material exchange with environment, controlled thermal release, suppression of degradation and large surface area [9, 10], which are very expected in the fields of solar photocatalysis [11, 12] and manufacture of heat transfer fluids [13, 14]. Composite PCMs prepared by using porous matrixes are dependent on the capillary force, hydrogen bonding interactions and interfacial adhesion to achieve leakage-proof [15, 16]. Matrixes such as porous inorganic clay (attapulgite [17], kaolinite [18], silica [19], diatomite [20], halloysite [21] and perlite [22]) and carbon-based adsorbents (carbon foam [23], expanded graphite [24] and grapheme aerogel [25]) with lightweight, stable and compatible traits can enable PCMs to adjust their density and thermal conductivity to practical needs, and make it possible to fabricate the

composites into any desirable shapes. Despite the superiority of the FSPCMs, some defects need to be considered. For instance, the microencapsulated PCMs present powder-like shape and easily get brittle under external pressure [26, 27], which are difficult to be applied in a package-free way. The FSPCMs based on porous carbon matrix demonstrate strong rigidity at low temperature but become very fragile as the PCM goes through solid-liquid phase change [28, 29]. How to install the FSPCMs in confined thermal energy storage units with minimized contact resistance and damages remains a big problem.

Shape memory property is a quality of materials that can enable materials to fix the deformed shape and recover to the original shape upon exposure to external stimulus [30, 31]. Conventionally, materials with shape memory property have two-phase structures: a switching phase which demines the shape transition and a permanent phase that is responsible for memorizing the initial shape [32]. Inspired by this property and the structural feature of the shape memory materials, it is expected that physical blending PCMs with the shape-stabilized matrixes that possess good elasticity may introduce shape variation ability to FSPCMs and further ensure accurate installations of them. In recent studies, composites with PCM (paraffin wax) serving as the switching phase and melamine foam as the permanent phase have been developed, and good form-stability as well as shape-fixing and recovery properties were found for them when they were installed in electronic devices [33] and building roof [34]. FSPCMs prepared by using epoxy resins-based covalent-noncovalent interpenetrating network to trap the liquid PCMs (polyethylene glycols) and act as the permanent phase to endow the yielded FSPCMs with shape memory property was also reported [35]. Although above strategy has realized the successful installation of FSPCMs in limited places, how to precisely control the shape-fixing and recovery process has not yet been considered. Besides, the prevention of cracks of these materials especially during the repeated shape deformation and recovery processes and the long-term resistance to mechanical damages still stay unsure. Developing

novel kinds of FSPCMs with both controllable shape memory property and healable characteristics to resist damages are quite desirable.

Polymers with crystalline segments of PCMs bounded on their skeletons are a newly developed type of solid-solid phase change materials. With the assistance of the crystalline chains, this type of materials is capable of phase transitions and possess heat storage capacity. So far, the reported solid-solid phase change polymers include polyurethane and polyurethane acrylate with the segments of polyethylene glycol located in the backbones [36-39] and epoxy-based polymers with the segments of 1-octadecanethiol grafted on the side chains [40, 41]. These materials not only possess good heat storage property but also exhibit thermal-induced flexibility and high compatibility with organic solid-liquid PCMs. Considering the special properties of these polymers, if they are acting as the permanent phases for the shape memory FSPCMs, the shape deformation or recovery would at least have two stages. The first stage is the thermal activation of the flexibility of the permanent phase and the second stage is shape variation stimulated by the switching phase. Consequently, the shape memory behaviours of the FSPCMs could be controllable. Besides, the good compatibility of the solid-solid phase change polymers with solid-liquid PCMs depends on the strong interactions between the crystalline segments and PCMs. These interactions as well as the solid-liquid phase transitions of PCMs in confined micro-scale regions may introduce strong self-repairing effects when the FSPCMs come across fractures [42].

Herein, we demonstrated the effectiveness of the above-mentioned new strategy regarding the achievement of controllable shape memory and self-healing properties for FSPCMs. A novel kind of FSPCMs based on blending ethylene glycole distearate (EGDS), which is the solid-liquid PCM, and epoxy-based polymer with segments of stearic acid (SA) bounded on the side chains were prepared. Notably, the SA segments in the polymer had similar structure to EGDS, which not only introduced crystalline part and made the polymer to be a solid-solid

phase change polymer but also ensured tight interactions between the polymer network and EGDS. Therefore, this epoxy-based polymer could act as both the shape-stabilized matrix and permanent phase for controllable shape memory. The structures and properties of the resultant FSPCMs were systematically characterized, and multiple functions of thermal regulation, shape memory with stepwise controllable character and self-healing were exhibited by the as-prepared materials. The composite FSPCM derived from current strategy not only showed good potentials in industrial uses but also implied a new avenue to develop multifunctional smart PCMs.

2. Experimental section

2.1 Materials

Diglycidyl ether of bisphenol A (DEGBA, purity: ≥85%, Mn: 340.42, mole per mass of epoxy group: 0.00587mol/g) was purchased from Aladdin Reagent Ltd. Stearic acid (SA, purity: 99%) was provided by Sinopharm Chemical Regent Co., Ltd. Benzyldimethylamine (BDMA, 99% purity) offered by Aladdin Reagent Ltd. was selected as the catalyst of epoxy-acid reaction. Cationic photoinitiator and photosensitizer with product numbers of PAG30101 and PSS306 from Changzhou Tronly New Electronic Materials Co., Ltd. (China) were used for photopolymerization of epoxy resin. Ethylene glycole distearate (EGDS, purity: ≥95%) was obtained from Guangzhou Daoming Chemical Co., Ltd.

2.2 Synthesis of SA-partially capped DEGBA

Stoichiometric amounts of SA (0.1 mol) and DEGBA (0.1 mol) were mixed at 80 °C until a homogenous solution was obtained, followed by adding BDMA (1wt% of DEGBA) dropwise within 1 h. After that, the epoxy-acid reaction was performed at 80 °C for 1 h, subsequently at

90 °C for 5 h. The resulting product was referred to be SA-partially capped DEGBA. The synthetic routes of SA-partially capped DEGBA are shown in Fig. 1 (Step 1).

2.3 Synthesis of EP/EGDS composite FSPCMs

SA-partially capped DEGBA, PAG30101 and PSS306 were mixed together with a mass ratio of 93/6/1 at 50 °C to form a transparent solution. Then, the solution was heated to 70 °C, followed by adding EGDS. The mass ratios of this solution to EGDS were 90/10, 80/20, 70/30, 60/40 and 50/50. After stirring at 70 °C for 1 h, the mixture was poured into a glass pool with a depth of 300 μm and exposed to 365 nm UV radiation at 50 °C for 30 min with a light-emitting diode (LED) array. The radiation intensity of the UV light was 100 $mW \cdot cm^{-2}$. The obtained samples were labelled as EP/EGDS-x composite PCMs according to the content of EGDS (x=10, 20, 30, 40 and 50). The sample synthesized without EGDS was the crosslinking product of the SA-partially capped DEGBA and named as EP. The preparation process of EP/EGDS composite can be seen in Fig. 1 (Step 2).

2.4 Instrument and measurements

Fourier transform infrared (FT-IR) experiments were carried out using a Nicolet 6700 FT-IR spectrophotometer (Thermo Fisher Scientific Inc., USA). Each sample was scanned 32 times in the wavenumber of 4000-500 cm^{-1} and the corresponding infrared spectrogram was obtained in an absorbance mode.

X-ray diffractometer (XRD) tests were conducted to characterize the crystalline properties of the FSPCMs on an X-ray diffractometer (D8 Advance, Bruker, Germany). Polarizing optical microscopy (POM) observation performing on a polarizing optical microscope (Scope A1, Zeiss, Germany) was also employed to provide more information of the crystallization features.

Scanning electron microscopy (SEM) observation was conducted by a scanning electron microscope (SU-70, Hitachi, Japan). Before the tests, all the samples were broken in liquid nitrogen and the obtained fracture surfaces were coated with gold to improve the conductivity and prevent charging.

Differential scanning calorimetry (DSC) measurements were carried out to determine the phase change parameters of the samples. Dynamic scans were performed on a differential scanning calorimeter (Q200, TA Instrument, USA) from 0-90 °C at a speed of 5 °C·min^{-1} under nitrogen flow.

The leakage tests of the EP/EGDS composite PCM were conducted by observing the samples placed on a heating platform (BK946, Bakon Instrument, China) with the temperature increasing from 20 to 120 °C. This process was recorded by digital photographs. Each sample was weighed before and after the test in order to calculate weight loss.

The thermal performance of the FSPCMs during heat storage and release processes were studied. The selected samples with a temperature of 20 °C were suddenly placed on a heating platform at 70 °C for thermal energy storage. After the temperature reaching about 70 °C, the samples were then removed and released the stored energy by natural cooling. The temperature variations of each sample during the experiments were monitored by an infrared thermal-imaging camera (865, Testo, Germany).

Thermogravimetry (TG) measurements were carried out on a thermal gravimetric analyser (TGA-55, TA Instrument, USA) from 30-600 °C at a speed of 10 °C·min^{-1} under nitrogen atmosphere.

The thermo-induced shape memory properties of the as-prepared FSPCMs were evaluated by a rolling-recovery test. Detail procedures of this test are supplied in Supporting Information.

The thermal-activated self-healing property of the EP/EGDS composite FSPCM was tested by following a breaking-healing procedure. The breaking process was performed under

ambient temperature and the self-healing behaviours of the samples were observed when 120 °C heating treatment was applied. Detailed procedures of these tests are given in Section 3.6.

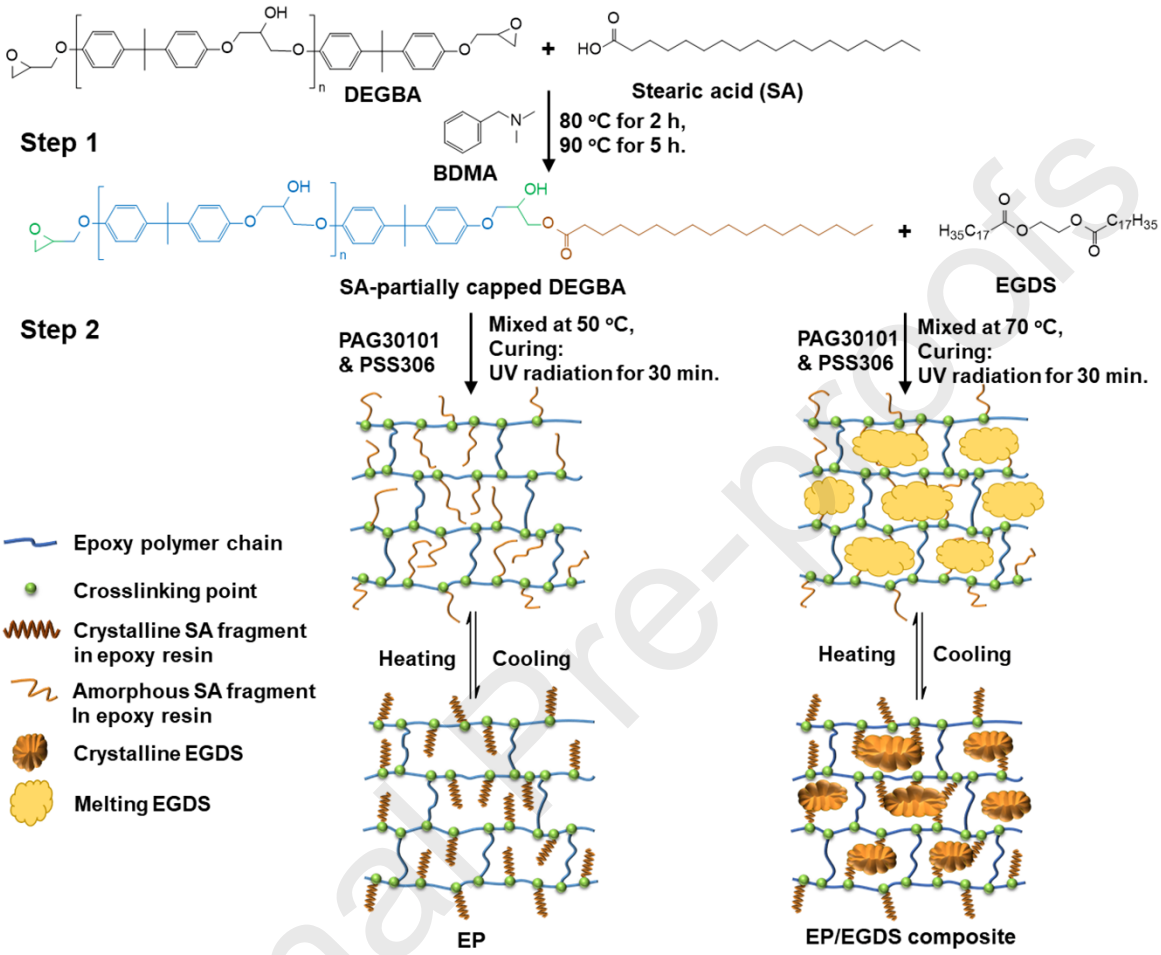

Fig. 1 Synthesis procedures of SA-partially capped DEGBA and EP/EGDS composite PCM.

3. Results and discussions

3.1 Synthesis and characterization of SA-partially capped DEGBA

The SA-partially capped DEGBA was synthesized based on an epoxy-acid reaction, and the synthesis progress was monitored using FT-IR. In the initial stage of the synthesis (t = 0), the reaction system was a simple mixture of SA and DEGBA, and all the characteristic peaks of the two raw materials given in Fig. 2(b) can be found in the spectra of the system (Fig. 2(a)).

Examples of those peaks include the 1701 cm^{-1} peak which belongs to the stretching vibrations of C=O in carboxyl groups in SA [43], and the peaks at 1608 cm^{-1} and 913 cm^{-1} assigned to the C=C stretching vibrations in benzene ring and stretching vibrations of C–O–C in epoxy groups in DEGBA [44], respectively. As the reaction proceeded, different changes of these peaks occurred. The intensity of the 1701 cm^{-1} peak decreases gradually, whereas a new peak at 1735 cm^{-1} representing stretching vibration of C=O in ester groups emerges and presents a time-dependent rising intensity. These phenomena are consistent with the acid-ester conversion and prove that the SA segments were successfully grafted on the epoxy resin. The intensity of the 913 cm^{-1} peak demonstrates a decreasing trend while a broad peak at 3455 cm^{-1} becomes obvious after the reaction (shown in Fig. 2(b)) due to the open-ring of the epoxy groups. Besides, for the 1608 cm^{-1} peak, very slight changes are observed, indicating the inactive behaviours of benzene ring during the reaction process.

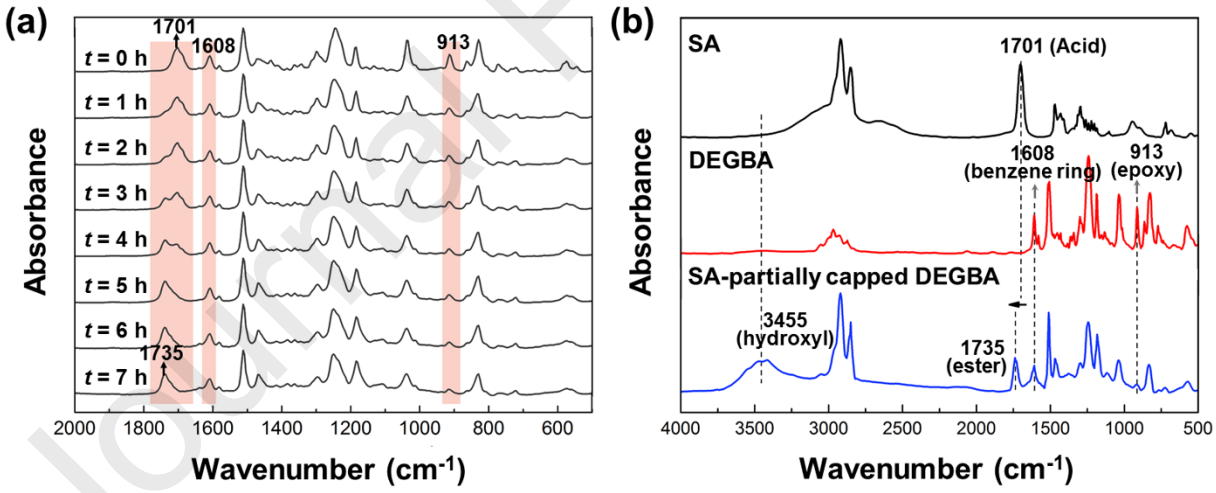

Fig. 2 FT-IR spectra of (a) the time-dependent epoxy-acid reaction system and (b) the SA, DEGBA and SA-partially capped DEGBA.

The epoxy conversion of DEGBA corresponding to different stages of the epoxy-acid reaction based on calculations of the areas of 913 cm^{-1} and 1608 cm^{-1} peaks are quantitatively

displayed in Fig. S2. The acid-ester conversion obtained through determinations of the acid values of the reaction system is also presented in the same figure. Complete conversion of the carboxyl groups was achieved after about 7 h when the acid-ester conversion reached 0.99, which agrees well with that no 1701 cm^{-1} peak was detected in the FT-IR test of the reaction product. The end of the epoxy-acid reaction, therefore, is revealed. About 0.52 conversion of epoxy groups in DEGBA was found at the same time. This value is a little higher than the theoretical obtained result (which is 0.5) possibly owning to the self-curing among DEGBA. Moreover, the DSC investigations (Fig. S3) show that phase transition peaks at around 30-35 °C are found for the reaction product, which is very different from SA and DEGBA. This could be ascribed to the phase change of the SA segments grafted on the epoxy resin. All these results confirm that the DEGBA molecular has been successfully capped with SA at its extremes and the SA-partially capped DEGBA were obtained.

3.2 Structure characterization of EP/EGDS composite PCMs

The FT-IR spectra of EGDS, EP/EGDS composite and EP are shown in Fig. 3(a). In comparison to the SA-partially capped DEGBA, both EP and the EP/EGDS composites show no peak at 913 cm^{-1} and the intensities of the peaks at around 3455 cm^{-1} are all very slight, suggesting that the crosslinking reaction among the SA-partially capped DEGBA was performed completely. The peaks at 2918 cm^{-1} and 2854 cm^{-1} are resulted from the stretching vibrations of C–H in $–CH_3$ and $–CH_2–$ groups, respectively [45]. The C–H bending vibrations of $–CH_2–$ and $–CH_3$ appear at 1459 cm^{-1} and 1384 cm^{-1} [36]. The peaks of stretching vibrations of C–C and in-plane rocking vibration of C–H are observed at 1174 cm^{-1} and 721 cm^{-1}, respectively. Above peaks are detected in all the presented samples, confirming the existence of long alkyl chains in their structures [46]. The stretching vibration of C=O is seen at 1735 cm^{-1}, which belongs to the ester groups in both EGDS and EP with SA segments. The peaks at

1608 cm^{-1} and 1511 cm^{-1} representing the C=C stretching vibration bands of the benzene ring, as well as the peak at 824 cm^{-1} in response to the C–H out-plane bending vibration of the benzene skeleton [41, 47], are found for the EP/EGDS samples. The C–O stretching vibration of aromatic ether at 1235 cm^{-1} [41] is also observed, which is consistent with the structure of EP. With the rise of the EGDS content (from 0 to 50 wt.%), the mass fraction of EP decreases and a gradual reduction in the intensities of the benzene ring-related characteristic peaks is noticed. By analysing the spectra of the EP/EGDS composites, all the characteristic peaks of EGDS and EP can be found and no significant new peak is detected, proving that there was no chemical interaction between EGDS and EP in the composites.

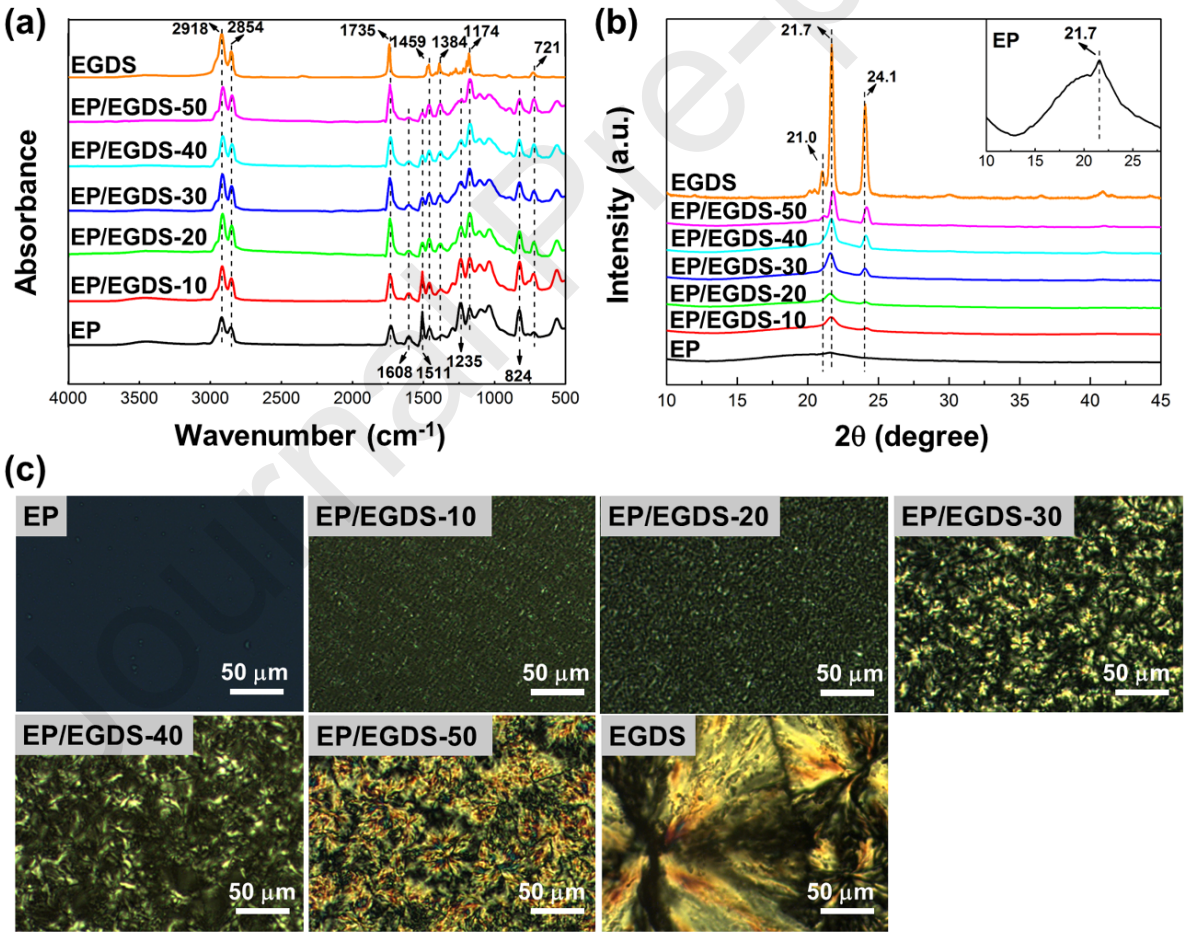

Fig. 3 Illustration of (a) FT-IR spectra, (b) XRD images and (c) POM spectra of EP, EGDS and EP/EGDS composite.

Fig. 3(b) demonstrates the XRD results of above samples to further analyse the interactions between EGDS and EP in the composite based on their crystalline information. A relatively broad and smooth peak at around 20° for EP corresponded to the amorphous epoxy polymer [41, 48] is presented (shown in the inserted figure). There is also a small sharp diffraction peak at 21.7° for EP, indicating the formation of crystalline side chains in the polymer network. The peaks appear at 21.0°, 21.7° and 24.1° are the diffraction peaks of crystalline phase of EGDS which were originated from the ordering of the long alkyl chains. For the EP/EGDS composite, all the characteristic diffraction peaks of EGDS are observed. With the rise of EGDS content in the composite, the intensities of the three peaks increase correspondingly. Besides, it should be noted that, in the XRD diagrams of the composite, the smooth peak of EP at 20° as well as the sharp crystalline peak is greatly covered up by the diffraction peaks of EGDS due to the close locations, making them very difficult to be identified even in the case when 90 wt.% EP exists. Above results suggest that the crystalline structures of EGDS were not destroyed while blending with the epoxy crosslinking network, further confirming that there was only a physical interaction between EGDS and epoxy polymer matrix.

Moreover, the POM observation was conducted to confirm the crystallinity of the as-prepared materials. In Fig. 3(c), all the samples exhibit birefringence in the POM spectra due to the existence of crystalline structures, which are consistent with the XRD results. However, the birefringence phenomena are quite different for those samples. For EP, the birefringence signals are very weak (See magnification image in Fig. S4) because of the low degree of crystallinity of the SA fragments resulting from the suppression of the polymer network. With the rise of the EGDS content, the crystalline domains in the composite increase. The pristine EGDS presents completed spherulite and the typical maltese cross is observed. It should be noted that the crystalline domains in EP/EGDS composites is uniformly dispersed in the

amorphous areas. This phenomenon could be ascribed to the good compatibility of the epoxy-based polymer with EGDS, which is also the result of the existence of the SA segments on the network of the polymer.

3.3 Form-stable property of EP/EGDS composite PCMs

The form-stable property of PCMs is of vital importance due to it, to some degree, determines how these materials can be practically used. Here, the form-stability of the EP/EGDS composite PCM was characterized by leakage tests. In Fig. 4(a), all samples can maintain solid state in the initial stage of the tests when the temperature is 20 °C. As the temperature gradually increases, solid-liquid phase transition of pristine EGDS occurs and then the liquid EGDS permeates into the papers, whereas no obvious leakage is observed for the film samples of EP and EP/EGDS composites even the temperature reaches 120 °C (much higher than the melting point of EGDS). Fig. 4(b) summarizes the weight loss of the samples after being heated at 120 °C for 1 h. The weight losses of EP and the EP/EGDS composite with EGDS content lower than and equalling to 30 % are determined to be zero. As for the samples of EP/EGDS-40 and EP/EGDS-50, the weight losses are 0.48 % and 1.14 %, respectively. The slight increasing trend of the weight loss corresponding to the increased loading of EGDS indicates that it was EP immobilized the liquid EGDS and imparted the EP/EGDS composite with leakage-proof property. A conclusion that the EP/EGDS composite could be a good FSPCM is confirmed. It is also noteworthy that when the mass fraction of EGDS exceeds 50 %, the EP/EGDS composite is difficult to prepare due to the overload of EGDS which lowers the concentration of the crosslinking points and then leads to a low crosslinking degree of EP. Thus, the obtained EP/EGDS composite would hardly be kept in a solid shape and maintain form-stable.

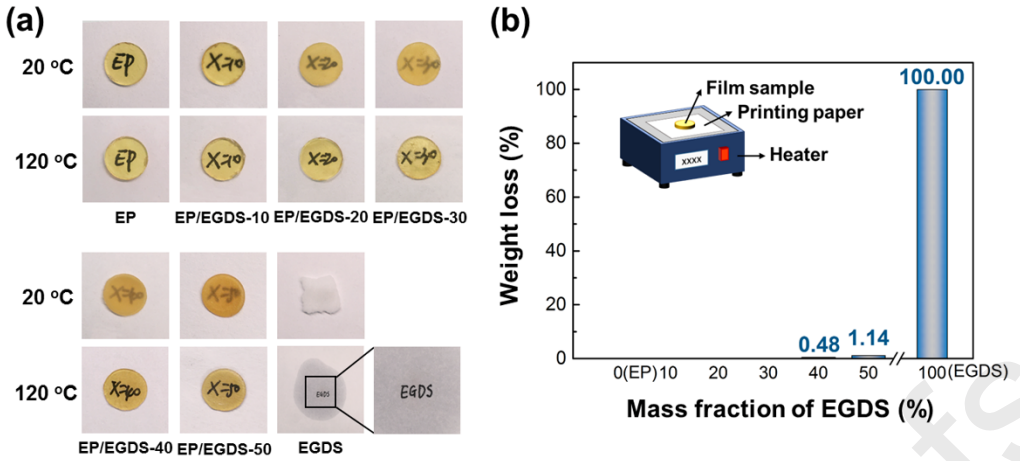

Fig. 4 Leakage performances of (a) EP, EP/EGDS composites and EGDS samples, and (b) weight loss of the samples after heating at 120 °C for 1 h. (The label of each sample is written on the printing paper)

Besides the form-stability, another phenomenon we notice in Fig. 4(a) is the EP film demonstrates very little opacity at 20 °C although with the attendance of crystalline SA segments. With the increase of the EGDS content in the composite, the transparency of the composite film becomes lower. This tendency mainly could be attributed to the decrease of refractive index which is determined by the crystalline properties of EGDS. As the temperature increases and reaches 120 °C, the crystalline EGDS transforms to amorphous state. Consequently, the composite films become transparent.

To improve our understanding of how the EP/EGDS composite perform form-stable behaviours and have a knowledge of the microstructures of the composite, SEM observations were employed. As shown in Fig. 5(a), there are two phases constituted EP in micro-scales (just as the XRD and POM results indicate): a continuous phase representing the amorphous polymer (black flat regions) and a dispersion phase which is the crystalline SA segments with lamellar shapes. Because the content of the SA segments in EP was low and the crystallization of the SA segments was suppressed by the polymer network, small amount of lamellar structures is found. When 10 wt.% EGDS is composited with EP, lamellar crystals still are observed but the

amount of them are larger due to the crystalline EGDS presented similar shapes of crystals. Moreover, because the SA segments and EGDS possess same long chain structures, the EGDS crystals could be uniformly mixed with the crystalline SA segments. The restrictions of those crystals within the regions surrounded by the polymer phase could explain the immobilization of EGDS at liquid state. As for the composite with EGDS mass faction of 20-50 %, the crystallinity degree of the composite increased and lamellar crystal bundles appear in the polymer network, indicating the formation of spherulites. Typical patterns of crystal bundles are seen in EP/EGDS-50 sample. In Fig. 5(b-f), uniform distribution of the crystalline structures in the polymer network is observed for the composite samples. This result along with that from the POM analysis confirm a good compatibility between the as-prepared EP and EGDS.

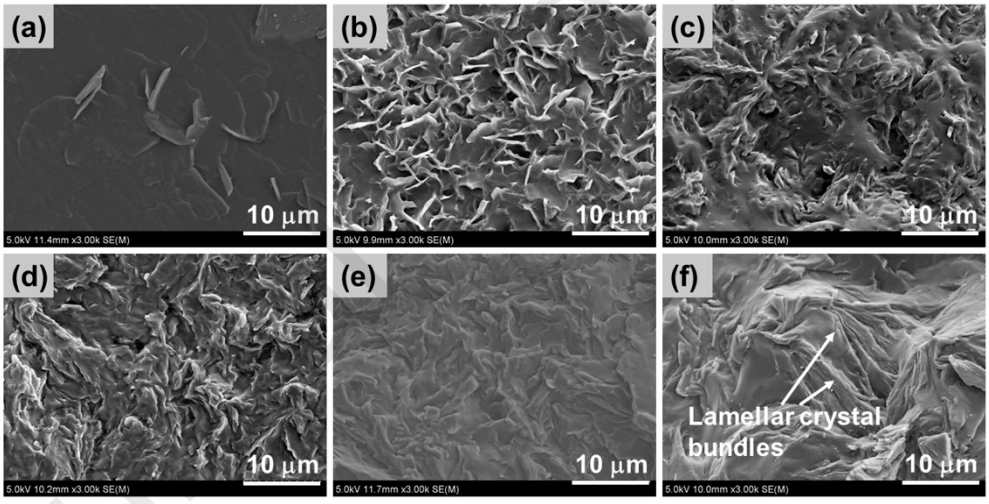

Fig. 5 SEM images of fractured interface of (a) EP, (b) EP/EGDS-10, (c) EP/EGDS-20, (d) EP/EGDS-30, (e) EP/EGDS-40 and (f) EP/EGDS-50.

3.4 Thermal analysis of EP/EGDS composite FSPCMs

Thermal property measurements of EP, EGDS and EP/EGDS composite by using DSC are demonstrated in Fig. 6. As it shows, EGDS exhibits two DSC peaks during melting or freezing process. The two melting peaks are located at 43.6 °C and 59.4 °C and the two freezing peaks

are found at 44.4 °C and 56.3 °C. The minor peaks at lower temperatures might be attributed to the melting and freezing of the crystal phase derived from heterogeneous nucleation, while the strong peaks possibly were caused by the phase changes of the crystal phase yielded based on homogeneous nucleation. Here, we define the onset temperatures of the major peaks at 59.4 °C and 56.3 °C as the melting and freezing temperatures of pristine EGDS, respectively. Only one single peak at 23.7 °C in the endothermic curve of EP and one single peak at 16.7 °C in the exothermic curve corresponding to the melting and crystallization of the SA segments, respectively, are detected. Therefore, 23.7 °C and 16.7 °C are defined to be the melting and freezing temperatures of pristine EP. When the EGDS is incorporated into the skeleton of EP, it is interesting that the melting and freezing temperatures of EP increase in comparison to pristine EP, whereas the phase transitions points of EGDS drop as compared to pristine EGDS. To understand these phenomena, one point to know is the SA segments in the structure of EP would interact with EGDS. The EGDS crystals which possess higher melting point than EP in the composite could, on one hand, suppress the flexibility of the SA segments during the melting process of EP, and on the other hand, act as a nucleating agent to accelerate the crystallization of the SA segments during EP's crystallization process. Consequently, upward shifts in the melting and freezing temperatures of EP could be obtained. As for EGDS in the composite, during the melting process of this material, the SA segments bounded on the polymer network would become soft first and destroy the crystal domain of EGDS, making the EGDS crystals more vulnerable. As it comes to the freezing process of EGDS in the composite, the polymer network might block the spreading of the seed crystals, leading to great difficulties in triggering the crystallization of EGDS. Hence, it is no surprising that downward shifts of the melting and freezing temperatures of EGDS in the composite. With the increased content of EGDS in the composite, the interactions between the SA segments and EGDS would be enhanced. These might explain the phenomena in Fig.6(c) and (d) that the melting and

crystallization temperatures of the EP/EGDS composite all present rising trends with the increase of EGDS mass fraction.

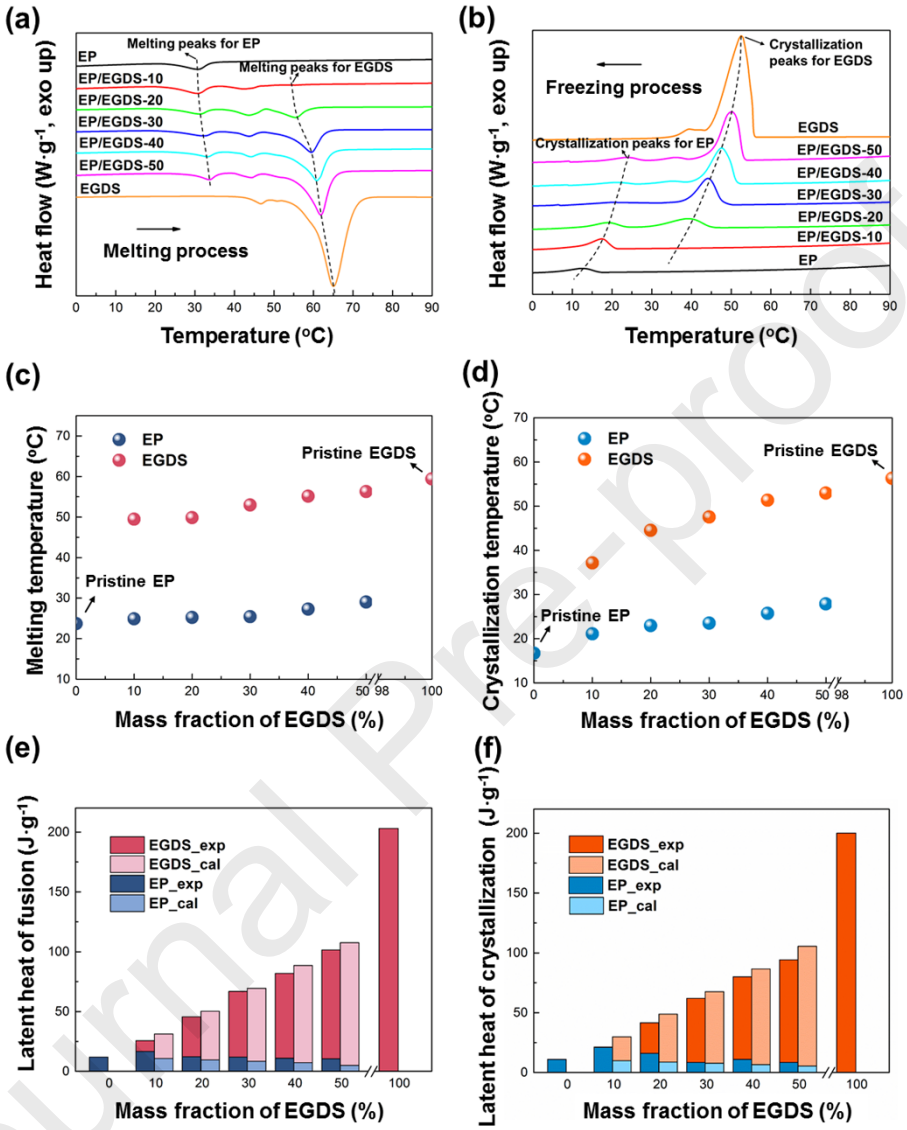

Fig. 6 DSC analysis of EP, EGDS and EP/EGDS composite: (a) heating and (b) cooling curves, (c) melting and (d) freezing temperatures, (e) latent heat of fusion and (f) crystallization.

Since there are two separated phase transitions during the heating/freezing process of the EP/EGDS composite PCM, the phase change latent heat of the composite is comprised of two portions. Fig. 6(e) and (f) demonstrates how the experimentally determined phase change

enthalpies of EP and EGDS parts constitute the latent heat of the composite. The theoretically obtained latent heat of EP part and EGDS part in the composite based on a speculation that their values are positively related to the mass fractions of EP and EGDS in the composite are also given. The melting and freezing latent heat of pristine EP are determined to be 12.1 $J \cdot g^{-1}$ and 11.0 $J \cdot g^{-1}$, and the corresponding values for pristine EGDS are 203.1 $J \cdot g^{-1}$ and 200.0 $J \cdot g^{-1}$. One thing to notice is the latent heat of EP part in the composite obtained from experiments is at least 12 % higher than that from calculations. The causes might be the existence of EGDS decreased the crosslinking density of EP, which further enlarge the phase change enthalpy of EP in the composite [49]. Besides, the determined latent heat of EGDS part in the composite is lower than the calculation result. According to the discussions concerning similar phenomenon in previous study [41], it could be due to a certain amount of EGDS were dissolved in the epoxy matrix and the phase change behaviours of this amount of EGDS were restricted.

The thermal energy storage and release performances of the EP/EGDS composite FSPCMs were further investigated to evaluate their potentials of thermal regulation. During the testing period, thin film samples of EP and EP/EGDS-30 composite were suddenly placed on a 70 °C heating plate for 40 s, and then quickly removed for natural cooling. An infrared thermal imager was employed to directly observe the thermal behaviours of the samples and monitor the transient average temperature of the films. As shown in Fig. 7, the first 10 s allows the temperatures of the two samples to increase at a nearly same speed and then reach around 50 °C. After that, discrepancies occurs and the temperature increasing speed of the EP/EGDS composite sample is degraded. The gap between the temperature vs. time curves of the two samples given in Fig. 7(c) clearly demonstrates how the composite moderate the thermal shock during the following 10 s period, which could be ascribed to the melting transition of EGDS in the composite. Both of the two samples would reach thermal equilibrium states at about 68 °C when the heating process finished. The cooling curves of EP and the EP/EGDS composite begin

to present divergent downward tendencies at about 40 °C. The sample of EP experiences a sharp temperature drop from 40 °C to 30 °C, whereas a comparatively slow temperature decreasing trend is found for the composite for this temperature interval. This phenomenon could be originated from the crystallization of EGDS in the composite. Above results indicate that the EP/EGDS composite possessed great abilities to resist thermal and cold shocks and the FSPCM films could be potentially applied as smart thermal regulation coating for electric circuits or window glass.

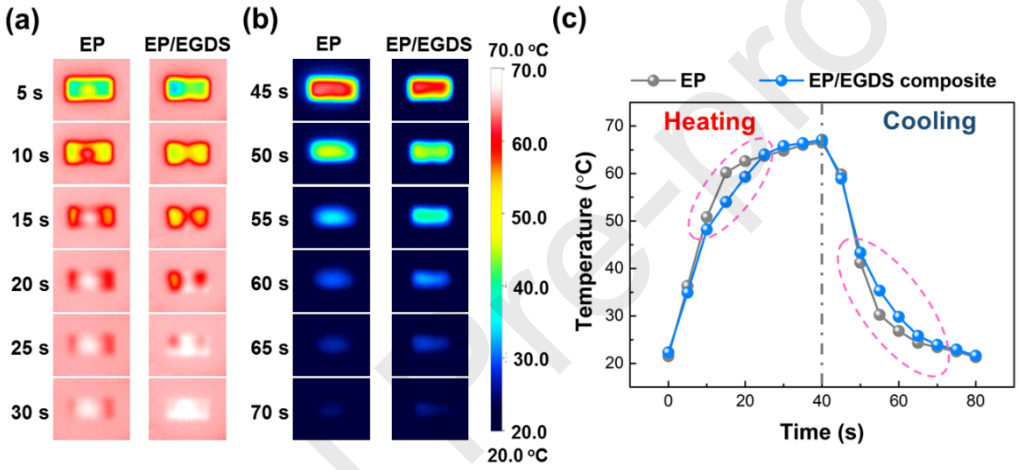

Fig. 7 Thermal energy storage/release performances of EP and EP/EGDS-30 composite FSPCM: infrared images recorded during (a) heating and (b) cooling processes, and (c) the corresponding temperature history curves.

3.5 Reliability evaluation of EP/EGDS composite FSPCM

Evaluating the reliability of the EP/EGDS composite is necessary due to it can enhance our understanding of the capabilities of this FSPCM to resist high temperature and degradation resulted from long-term cyclic uses, and further facilitate the material application. Fig. 8 demonstrates the TG and DTG curves of EP, EGDS and EP/EGDS composite. From 30 to 600 °C, pristine EGDS only comes across one-stage weight loss, whereas two-stage process is found

for EP. The two onset temperatures of the DTG peaks of EP are determined to be 180 °C and 352 °C, indicating the locations of two decomposition points of EP. Since the latter decomposition temperature of EP is very close to that of the crosslinking product of DGEBA (325 °C [40]), we could speculate that the second weight loss stage for EP was the consequence of the degradation of the epoxy based skeleton. And the first stage should be attributed to the lower thermal stability of the SA segment grafted in the structure of the polymer. The upper limit temperature for EGDS to stay thermal stable is 299 °C. This value is higher than the initial decomposition temperature of EP, indicating that EGDS possessed higher resistance against high temperature. As for the EP/EGDS composite, three-stage weight loss processes are identified for all the composite samples in the temperature range of 30-600 °C due to the different thermal stable behaviours of the two components in this FSPCM. With an increase in the EGDS content, the first stage of weight loss for the composite which might represent the decomposition of the grafted SA segments in EP becomes minor, while the second stage indicating the degradation of EGDS is getting obvious. In addition, higher initial decomposition temperature of the composite is achieved when the EGDS content is in a high level (Table S1). The possible reason could be the intermolecular forces between EGDS and the SA segments in EP that help slow down the thermal decomposition process of the grafted SA segments.

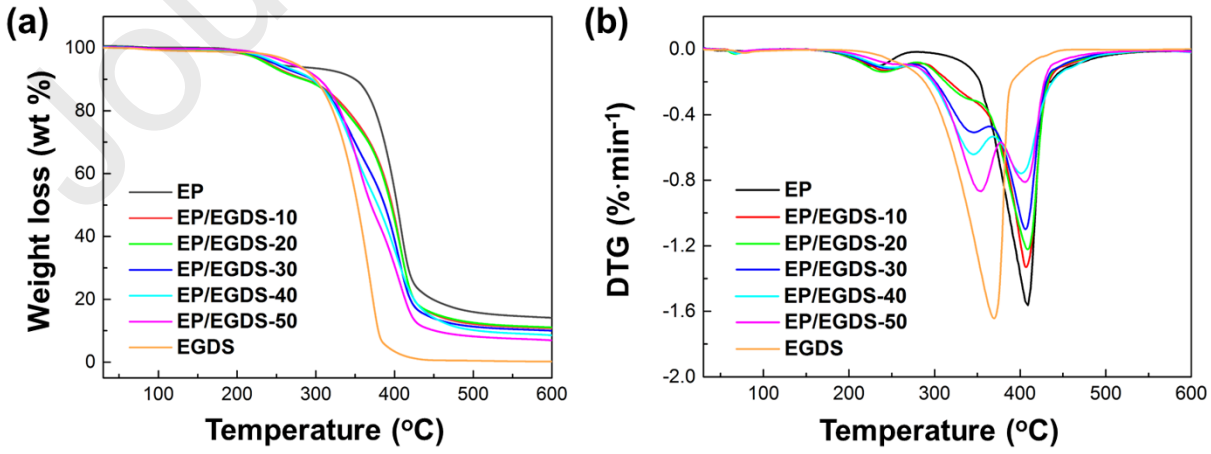

Fig. 8 TG analysis of EP, EGDS, and EP/EGDS composite: (a) TG and (b) DTG curves.

DSC curves of the EP/EGDS composites with different EGDS content before and after enduring 50 cycles of heating and cooling in a temperature range of -10-80 °C are compared in Fig. S5. The total latent heats of the samples derived from these curves are given in Table S2. As the figure indicates, all the composite samples present almost identical DSC curves before and after the thermal cycling. No obvious shift in the phase change temperatures are observed when these samples have been through 50 thermal cycles. The maximum loss of the total latent heat of the composite samples is determined to be less than 1.4 %. These results proved that the EP/EGDS composite FSPCM had a high stability for long-term cyclic thermal regulation uses.

3.6 Shape memory behaviour of EP/EGDS composite FSPCM

Fig. 9(a) demonstrates the reversible shape deformation and recovery behaviours of the film samples made of EP/EGDS-30 as an example. Obviously, the samples could easily be bended or rolled up regardless of their original shapes when the temperature is 70.0 °C (above the melting temperature of EP/EGDS-30). Good fixed shapes of the samples are observed when they are cooled to 20 °C (below the crystallization temperature of EP/EGDS-30). Considering EP as the permanent phase for shape memory of the composite had crystalline structures to enable phase transitions and possessed thermo-stimulated flexibility (Fig. S6), the as-prepared EP/EGDS composite can exhibit stepwise shape recovery behaviours. Fig. 9(b) quantitatively presents the shape recovery ratio of the composite film in a rectangle shape as a function of temperature. Obviously, there are three steps in the shape recovery ratio vs. temperature curve. The first step appears at around 33 °C which demonstrates a minor shape recovery movement of the sample. Due to the DSC peak of the EP part in the composite locates at close temperature positions, this shape recovery movement could be stimulated by the phase transition of the SA segments in the structure of EP. Moreover, based on the comparison of the POM spectra of the sample between 20 and 35 °C (Fig. 9(c)), very slight difference in birefringence patterns are

observed, indicating that no EGDS crystals were melted, which also reveal that only the phase transition of EP could be responsible for the shape recovery behaviour at this stage. The second step can be seen at around 45 °C and about 14 % shape recovery is found for the sample due to the melting of the EGDS crystal phase possibly produced through heterogeneous nucleation. The DSC peak located at the temperature interval 35-50 °C as well as the disappearance of a part of the birefringence pattern in POM spectra during this temperature range could prove this theory. The final step of the shape recovery of the composite film was driven by the solid-liquid phase transition of the EGDS crystal phase possibly yielded from homogeneous nucleation. 100 % of the shape recovery ratio is achieved when the phase change process of the composite completed. No signals of crystals are observed in the POM spectra when the temperature reached 70 °C. Above analysis suggests that the shape recovery process of the EP/EGDS composite FSPCM was handled by the three phase transitions of the FSPCM, and a precise control of the shape memory behaviours of the FSPCM could be realized by managing the temperature.

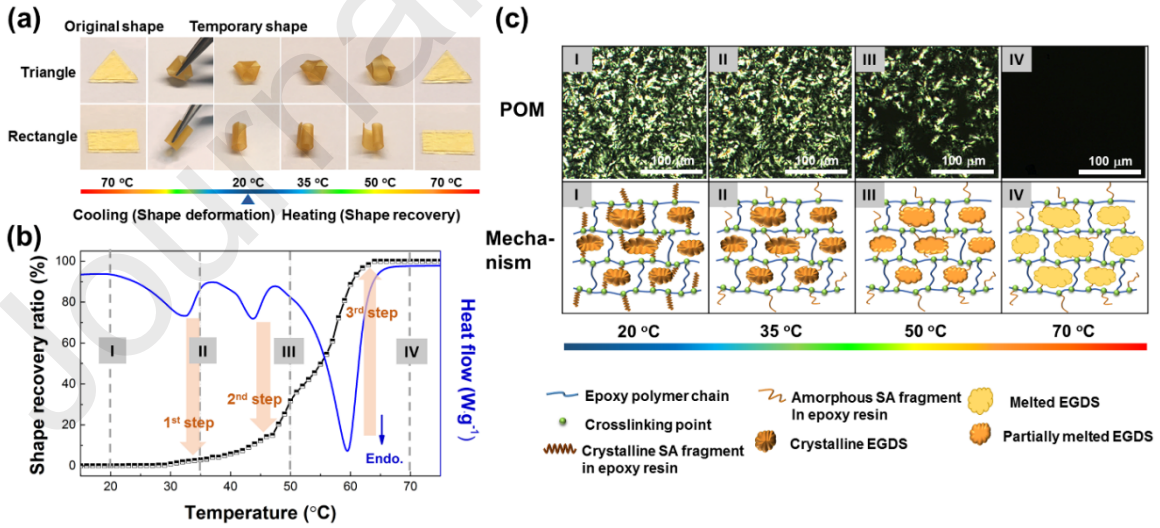

Fig. 9 Reversible shape deformation and recovery behaviours of EP/EGDS -30 FSPCM: (a) visual images, (b) shape recovery ratio as a function of temperature and (c) POM spectra and mechanism diagram at different shape recovery stages.

Fig. 10 displays how the shape recovery rate of the EP/EGDS composite FSPCM films varies with time when they are subjected to 70 °C. The film sample of EP/EGDS-10 recovers to its original straight shape very fast. The more EGDS concentration in the composite, the more time is consumed for a full shape recovery behaviour. As discussed above, the shape recovery of the FSPCM was triggered by the melting of the crystalline parts. With a rising content of EGDS, significant increments in the latent heat of fusion would occur to the FSPCM, and thus it would take more time for the film samples with higher EGDS concentration to achieve a complete melting. The phenomena observed in Fig. 10 also indicate that varying the loading content of EGDS in the composite is also an available option to control the shape memory behaviour of the EP/EGDS composite FSPCM.

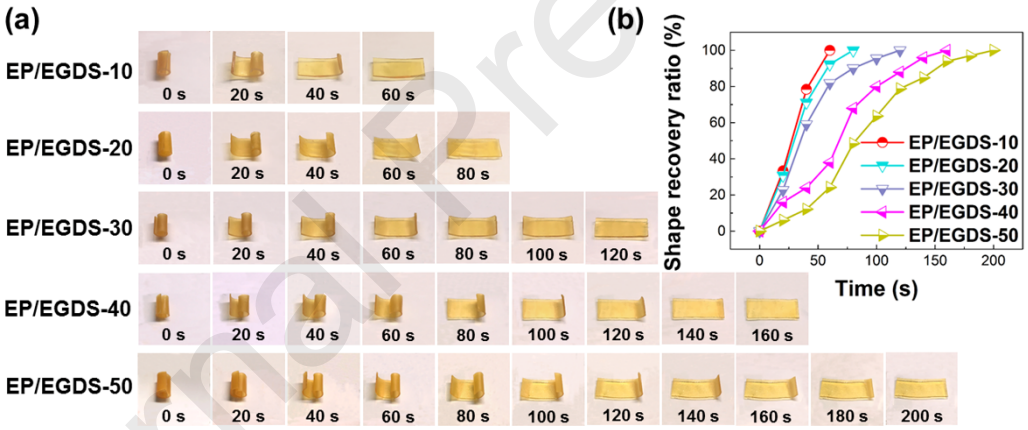

Fig. 10 Shape recovery of the EP/EGDS composite films: (a) visual images and (b) shape recovery ratio as a function of time.

3.7 Self-healing performances of the EP/EGDS composite FSPCM

Self-healing ability of the EP/EGDS composite FSPCM was evaluated by breaking a test sample into two pieces, followed by contacting the created two fracture surfaces under a 120 °C heating treatment. After 10 min, the sample was cooled to 20 °C. The test of the film sample of EP was also conducted for comparison. As it is seen in Fig. 11(a), the EP/EGDS composite

performs a good self-healing behaviour and the interfaces of the two fractures disappear almost completely after the test. Only very slight breaking mark on the surface of the composite sample is visible under the observation of a 3D digital microscope (VHX-950F, KEYENCE). The self-healed film composite sample could withstand certain external mechanical forces such as rolling. As for the EP film sample, the two broken pieces fail to adhere to each other. The adhesive force between the EP pieces is too weak to withstand the own weights of the pieces.

To explain the self-healing behaviour of the EP/EGDS composite, a schematic diagram of the possible healing mechanism is presented in Fig. 11(b). In the composite system, there might be at least five kinds of forces that pulled the fracture surfaces of the broken pieces of the composite sample together. These forces can be summarized as two categories. The first category exists in both EP and the EP/EGDS composite samples and comprised of (1-i) hydrogen bonds which are formed among the hydroxyl groups in the fracture surfaces of two different broken pieces, (1-ii) the van der Waals forces and (1-iii) the interactions among the soft SA segments when the temperature is above the melting point of EP. The second category of adhesive forces is closely related to EGDS, and includes two kinds of forces. First, due to the SA segments have similar structures to the EGDS, there would be a strong tendency of the soft SA segments to interact with the liquid EGDS. Second, according to the SEM and POM analysis, there are numerous separated micro-scale crystalline EGDS domains uniformly dispersed in the EP skeleton. When the temperature of the composite increases and reaches above the melting point of EGDS, these domains would become liquid zones. The EGDS liquid zones on the surface of the composite sample would tend to merge especially when the polymer phase surrounding them crack, and consequently the surfaces of the broken pieces would be soldered together. It should be noted that the second category of the forces dominated the self-healing behaviours of the EP/EGDS composite due to the fact the pristine EP film sample without the attendance of EGDS shows a poor self-healing ability. Besides above forces, from

the dynamic self-healing performance of the EP/EGDS-40 sample (Video. S1), we notice that the two pieces of broken sample automatically stretch and recovery to their original shape during heating due to the shape memory characteristic. These behaviours will help ensure close contacts between the two surfaces of the broken sample, which further facilitate the self-repairing effects.

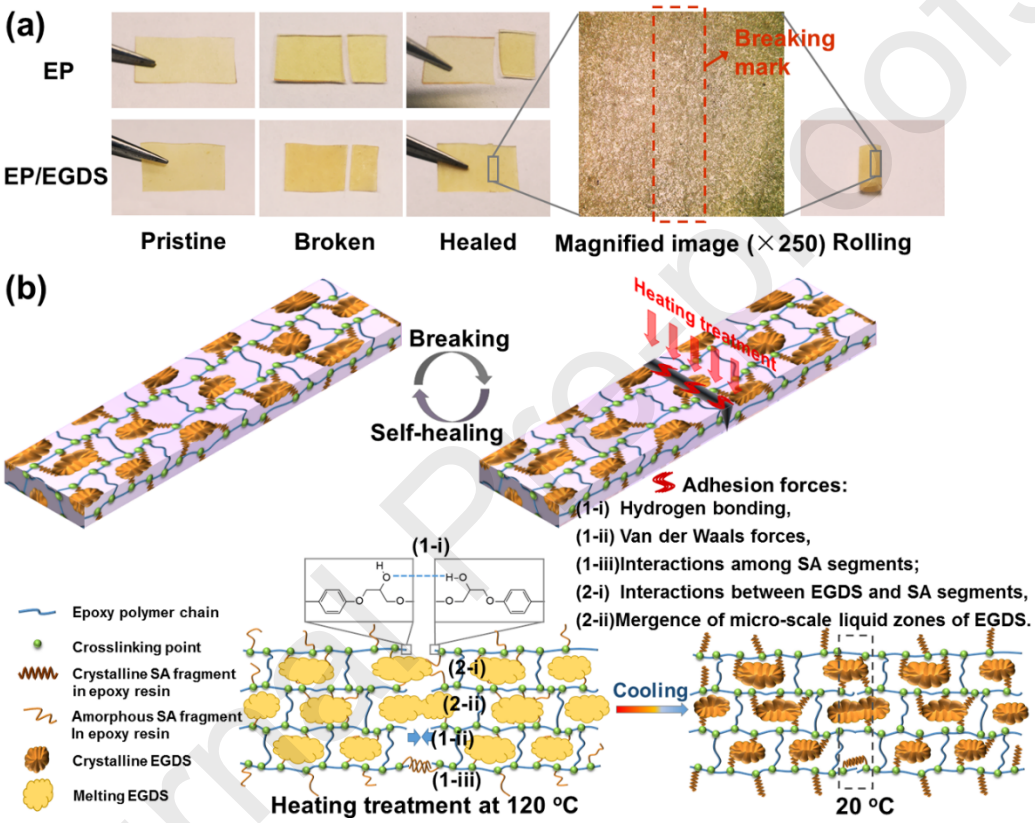

Fig. 11 Self-healing behaviours of EP/EGDS composite: (a) visual images of EP and EP/EGDS-40, and (b) schematic of healing mechanism.

4. Conclusion

In this work, we successfully prepared a novel composite FSPCM by confining EGDS within epoxy-based polymer with SA segments bounded on the side chains. In comparison to traditional FSPCMs, the two components of the composite could play

multiple roles: (i) EGDS works as a latent heat storage material for thermal regulation, a switching phase for shape transition and main adhesive medium for self-repairing; and (ii) epoxy-based polymer serves as shape-stabilized matrix and permanent phase for shape recovery. Structure and property characterization suggested a homogenous physical blending between EGDS and the polymer and desirable form-stable property was obtained by the composite owning to the SA segments increased the compatibility between EGDS and the polymer network. Moreover, the obtained FSPCM exhibited thermal regulation owning to the relatively large phase change enthalpy (around 101 $J \cdot g^{-1}$ for EP/EGDS-50). Good reliability of the FSPCM when the material maintained below 180 °C and was being through long-term repeated heating and cooling cycles were testified. Because of the multiple phase transitions introduced by both EGDS and the SA segments in EP, the FSPCM films presented controllable stepwise thermo-induced shape fixing and recovery behaviours. Besides, the EP/EGDS composite also perform thermo-activated self-repairing effect due to the solid-liquid transition of EGDS and the interactions between the SA segments and EGDS. Given the multiple abilities of the as-prepared material, our work can provide a promising FSPCM for thermal management of microelectronic devices and building glazing systems. Meanwhile, the strategy we used to develop the multifunctional FSPCM will have great prospects in guidance of imparting the FSPCMs with more smart properties.

Acknowledgment

This research was financially supported by the National Nature Science Foundation of China (51873108, 21908091), a Shenzhen Sci. & Tech. research grant

(JCYJ20180305124237416) and the National Key R&D Program of China (2018YFC1900603).

References

[1] Y. Tian, C.Y. Zhao, A review of solar collectors and thermal energy storage in solar thermal applications, Applied Energy 104 (2013) 538-553.

[2] L. Miró, J. Gasia, L.F. Cabeza, Thermal energy storage (TES) for industrial waste heat (IWH) recovery: A review, Applied Energy 179 (2016) 284-301.

[3] A.M. Khudhair, M.M. Farid, A review on energy conservation in building applications with thermal storage by latent heat using phase change materials, Energy Conversion and Managment. 45 (2004) 263-275.

[4] S.K. Sahoo, M.K. Das, P. Rath, Application of TCE-PCM based heat sinks for cooling of electronic components: A review, Renewable and Sustainable Energy Reviews 59 (2016) 550-582.

[5] M.M. Kenisarin, Thermophysical properties of some organic phase change materials for latent heat storage. A review, Solar Energy 107 (2014) 553-575.

[6] N. Zhang, Y. Yuan, X. Cao, Y. Du, Z. Zhang, Y. Gui, Latent Heat Thermal Energy Storage Systems with Solid–Liquid Phase Change Materials: A Review, Advanced Engineering Materials 20 (2018) 1700753.

[7] G. Abdeali, A.R. Bahramian, M. Abdollahi, Review on Nanostructure Supporting Material Strategies in Shape-stabilized Phase Change Materials, Journal of Energy Storage 29 (2020) 101299.

Journal Pre-proofs

[8] M.M. Umair, Y. Zhang, K. Iqbal, S. Zhang, B. Tang, Novel strategies and supporting materials applied to shape-stabilize organic phase change materials for thermal energy storage–A review, Applied Energy 235 (2019) 846-873.

[9] G. Alva, Y. Lin, L. Liu, G. Fang, Synthesis, characterization and applications of microencapsulated phase change materials in thermal energy storage: A review, Energy and Buildings 144 (2017) 276-294.

[10] E.M. Shchukina, M. Graham, Z. Zheng, D.G. Shchukin, Nanoencapsulation of phase change materials for advanced thermal energy storage systems, Chemical Society Reviews 47 (2018) 4156-4175.

[11] H. Liu, X. Wang, D. Wu, Tailoring of bifunctional microencapsulated phase change materials with CdS/SiO2 double-layered shell for solar photocatalysis and solar thermal energy storage, Applied Thermal Engineering 134 (2018) 603-614.

[12] L. Chai, X. Wang, D. Wu, Development of bifunctional microencapsulated phase change materials with crystalline titanium dioxide shell for latent-heat storage and photocatalytic effectiveness, Applied Energy 138 (2015) 661-674.

[13] G.H. Zhang, C.Y. Zhao, Thermal property investigation of aqueous suspensions of microencapsulated phase change material and carbon nanotubes as a novel heat transfer fluid, Renewable Energy 60 (2013) 433-438.

[14] X. Ma, Y. Liu, H. Liu, L. Zhang, B. Xu, F. Xiao, Fabrication of novel slurry containing graphene oxide-modified microencapsulated phase change material for direct absorption solar collector, Solar Energy Materials and Solar Cells 188 (2018) 73-80.

[15] P. Lv, C. Liu, Z. Rao, Review on clay mineral-based form-stable phase change materials: Preparation, characterization and applications, Renewable and Sustainable Energy Reviews 68 (2017) 707-726.

[16] J. Yang, L.-S. Tang, L. Bai, R.-Y. Bao, Z.-Y. Liu, B.-H. Xie, M.-B. Yang, W. Yang, High-performance composite phase change materials for energy conversion based on macroscopically three-dimensional structural materials, Materials Horizons 6 (2019) 250-273.

[17] M. Li, Z. Wu, H. Kao, Study on preparation, structure and thermal energy storage property of capric–palmitic acid/attapulgite composite phase change materials, Applied Energy 88 (2011) 3125-3132.

[18] J. Li, X. Zuo, X. Zhao, D. Li, H. Yang, Stearic acid hybridizing kaolinite as shape-stabilized phase change material for thermal energy storage, Applied Clay Science 183 (2019) 105358.

[19] J. Wang, M. Yang, Y. Lu, Z. Jin, L. Tan, H. Gao, S. Fan, W. Dong, G. Wang, Surface functionalization engineering driven crystallization behavior of polyethylene glycol confined in mesoporous silica for shape-stabilized phase change materials, Nano Energy 19 (2016) 78-87.

[20] A. Miliozzi, M. Chieruzzi, L. Torre, Experimental investigation of a cementitious heat storage medium incorporating a solar salt/diatomite composite phase change material, Applied Energy 250 (2019) 1023-1035.

[21] S. Thanakkasaranee, J. Seo, Effect of halloysite nanotubes on shape stabilities of polyethylene glycol-based composite phase change materials, International Journal of Heat and Mass Transfer 132 (2019) 154-161.

[22] C. Liu, C. Luo, T. Xu, P. Lv, Z. Rao, Experimental study on the thermal performance of capric acid-myristyl alcohol/expanded perlite composite phase change materials for thermal energy storage, Solar Energy 191 (2019) 585-595.

[23] K. Lafdi, O. Mesalhy, A. Elyafy, Graphite foams infiltrated with phase change materials as alternative materials for space and terrestrial thermal energy storage applications, Carbon 46 (2008) 159-168.

[24] H. Ghasemi Bahraseman, E.M. Languri, J. East, Fast charging of thermal energy storage systems enabled by phase change materials mixed with expanded graphite, Int J Heat Mass Tran 109 (2017) 1052-1058.

[25] P. Min, J. Liu, X. Li, F. An, P. Liu, Y. Shen, N. Koratkar, Z.-Z. Yu, Thermally Conductive Phase Change Composites Featuring Anisotropic Graphene Aerogels for Real-Time and Fast-Charging Solar-Thermal Energy Conversion, Advanced Functional Materials 28 (2018) 1805365.

[26] M. Li, J. Liu, J. Shi, Synthesis and properties of phase change microcapsule with SiO_2-TiO_2 hybrid shell, Solar Energy 167 (2018) 158-164.

[27] Z. Jiang, W. Yang, F. He, C. Xie, J. Fan, J. Wu, K. Zhang, Microencapsulated Paraffin Phase-Change Material with Calcium Carbonate Shell for Thermal Energy Storage and Solar-Thermal Conversion, Langmuir 34 (2018) 14254-14264.

[28] Q. Sun, H. Zhang, J. Xue, X. Yu, Y. Yuan, X. Cao, Flexible phase change materials for thermal storage and temperature control, Chemical Engineering Journal 353 (2018) 920-929.

[29] H.-y. Wu, R.-t. Chen, Y.-w. Shao, X.-d. Qi, J.-h. Yang, Y. Wang, Novel Flexible Phase Change Materials with Mussel-Inspired Modification of Melamine Foam for Simultaneous Light-Actuated Shape Memory and Light-to-Thermal Energy Storage Capability, ACS Sustainable Chemistry & Engineering 7 (2019) 13532-13542.

[30] A. Lendlein, S. Kelch, Shape-Memory Polymers, Angewandte Chemie International Edition 41 (2002) 2034-2057.

[31] Q. Zhao, H.J. Qi, T. Xie, Recent progress in shape memory polymer: New behavior, enabling materials, and mechanistic understanding, Progress in Polymer Science 49-50 (2015) 79-120.

[32] C. Liu, H. Qin, P.T. Mather, Review of progress in shape-memory polymers, Journal of Materials Chemistry 17 (2007) 1543-1558.

[33] J.-h. Jing, H.-y. Wu, Y.-w. Shao, X.-d. Qi, J.-h. Yang, Y. Wang, Melamine Foam-Supported Form-Stable Phase Change Materials with Simultaneous Thermal Energy Storage and Shape Memory Properties for Thermal Management of Electronic Devices, ACS Applied Materials & Interfaces 11 (2019) 19252-19259.

[34] H.-y. Wu, S.-t. Li, Y.-w. Shao, X.-z. Jin, X.-d. Qi, J.-h. Yang, Z.-w. Zhou, Y. Wang, Melamine foam/reduced graphene oxide supported form-stable phase change materials with simultaneous shape memory property and light-to-thermal energy storage capability, Chemical Engineering Journal 379 (2020) 122373.

[35] F. Luo, P. Yan, Q. Qian, H. Li, B. Huang, Q. Chen, K. Wu, M. Lu, Highly thermally conductive phase change composites for thermal energy storage featuring shape memory, Composites Part A: Applied Science and Manufacturing 129 (2020) 105706.

[36] X. Fu, Y. Xiao, K. Hu, J. Wang, J. Lei, C. Zhou, Thermosetting solid–solid phase change materials composed of poly(ethylene glycol)-based two components: Flexible application for thermal energy storage, Chemical Engineering Journal 291 (2016) 138-148.

[37] Z. Liu, B. Wu, X. Fu, P. Yan, Y. Yuan, C. Zhou, J. Lei, Two components based polyethylene glycol/thermosetting solid-solid phase change material composites as novel form stable phase change materials for flexible thermal energy storage application, Solar Energy Materials and Solar Cells 170 (2017) 197-204.

[38] Y. Zhang, J. Xiu, B. Tang, R. Lu, S. Zhang, Novel semi-interpenetrating network structural phase change composites with high phase change enthalpy, AIChE Journal 64 (2018) 688-696.

[39] Y. Meng, Y. Zhao, Y. Zhang, B. Tang, Induced dipole force driven PEG/PPEGMA form-stable phase change energy storage materials with high latent heat, Chemical Engineering Journal 390 (2020) 124618.

Journal Pre-proofs

[40] Q. Lian, K. Li, A.A.S. Sayyed, J. Cheng, J. Zhang, Study on a reliable epoxy-based phase change material: facile preparation, tunable properties, and phase/microphase separation behavior, Journal of Materials Chemistry A 5 (2017) 14562-14574.

[41] Q. Lian, Y. Li, A.A.S. Sayyed, J. Cheng, J. Zhang, Facile Strategy in Designing Epoxy/Paraffin Multiple Phase Change Materials for Thermal Energy Storage Applications, ACS Sustainable Chemistry & Engineering 6 (2018) 3375-3384.

[42] Y. Cheng, X. Xiao, K. Pan, H. Pang, Development and application of self-healing materials in smart batteries and supercapacitors, Chemical Engineering Journal 380 (2020) 122565.

[43] H. Zhang, X. Gao, C. Chen, T. Xu, Y. Fang, Z. Zhang, A capric–palmitic–stearic acid ternary eutectic mixture/expanded graphite composite phase change material for thermal energy storage, Composites Part A: Applied Science and Manufacturing 87 (2016) 138-145.

[44] H. Yamasaki, S. Morita, Temperature dependence of isothermal curing reaction of epoxy resin studied by modulated differential scanning calorimetry and infrared spectroscopy, Journal of Molecular Structure 1124 (2016) 249-255.

[45] D. Wu, W. Wen, S. Chen, H. Zhang, Preparation and properties of a novel form-stable phase change material based on a gelator, Journal of Materials Chemistry A 3 (2015) 2589-2600.

[46] R. Cao, Y. Wang, S. Chen, N. Han, H. Liu, X. Zhang, Multiresponsive Shape-Stabilized Hexadecyl Acrylate-Grafted Graphene as a Phase Change Material with Enhanced Thermal and Electrical Conductivities, ACS Applied Materials & Interfaces 11 (2019) 8982-8991.

[47] B. Tang, L. Wang, Y. Xu, J. Xiu, S. Zhang, Hexadecanol/phase change polyurethane composite as form-stable phase change material for thermal energy storage, Solar Energy Materials and Solar Cells 144 (2016) 1-6.

Journal Pre-proofs

[48] B. Wu, Y. Jiang, Y. Wang, C. Zhou, X. Zhang, J. Lei, Study on a PEG/epoxy shape-stabilized phase change material: Preparation, thermal properties and thermal storage performance, International Journal of Heat and Mass Transfer 126 (2018) 1134-1142.

[49] Y. Qin, K. Chen, H. Zhang, X. Luo, S. Liang, C. Tian, J. Wang, L. Zhang, Structure-property correlation of poly(ethylene glycol) based form stable phase change materials with different crosslinking structure, Solar Energy Materials and Solar Cells 203 (2019) 110192.

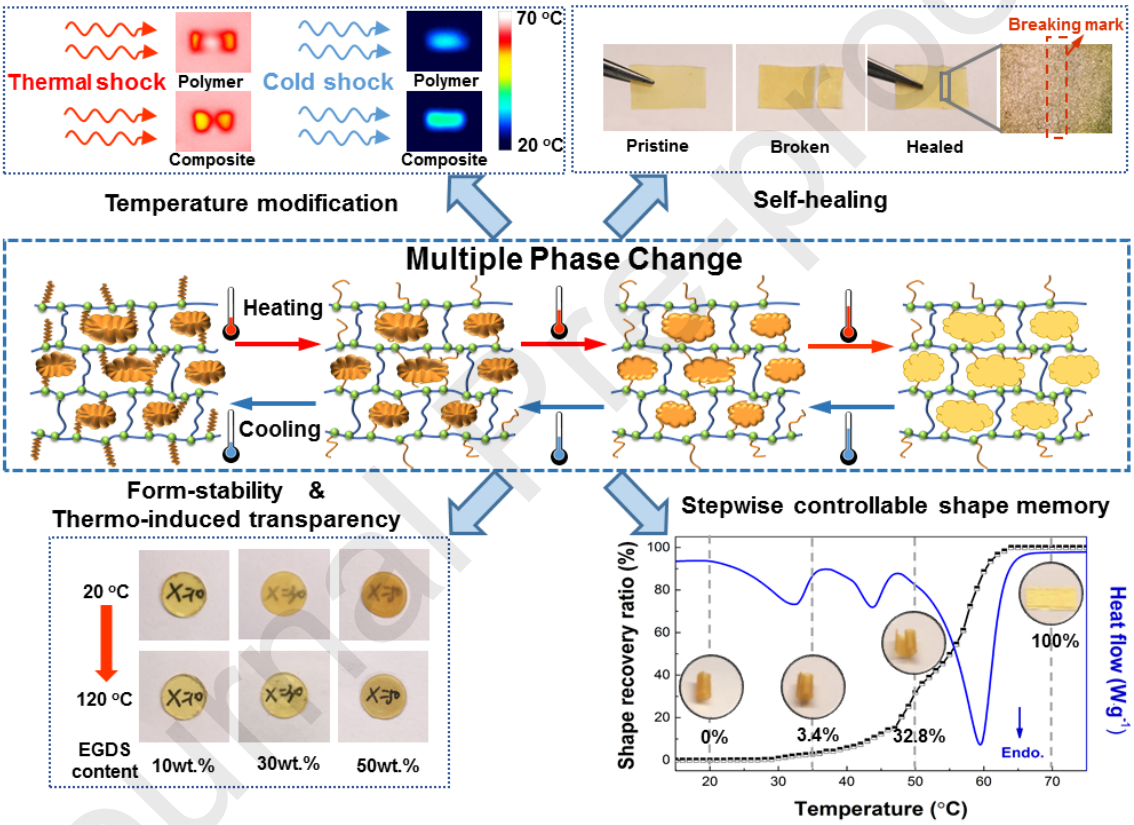

Highlights

- Novel epoxy composites for efficient thermal regulation were developed.
- Multiple phase transitions lead composites to perform controllable shape memory.
- Thermo-induced self-healing character is found for the composite.
- The composite shows excellent shape stability and thermo-sensitive transparency.